PHYSICAL REVIEW B **91**, 205117 (2015)

Dynamics of photogenerated nonequilibrium electronic states in Ar^+-ion-irradiated $SrTiO_3$

Dushyant Kumar, Z. Hossain, and R. C. Budhani*

Condensed Matter Low Dimensional Systems Laboratory, Department of Physics, Indian Institute of Technology, Kanpur 208016, India

(Received 11 March 2015; revised manuscript received 2 May 2015; published 18 May 2015)

A metallic surface is realized on stoichiometric and insulating (100) $SrTiO_3$ by Ar^+-ion irradiation. The sheet carrier density and Hall mobility of the layer are $\sim 4.0 \times 10^{14}$ cm^{-2} and $\sim 2 \times 10^3$ cm^2/Vs, respectively, at 15 K for the irradiation dose of $\sim 4.2 \times 10^{18}$ ions/cm^2. These samples display ultraviolet light sensitive photoconductivity (PC) which is enhanced abruptly below the temperature ($\approx$100 K) where $SrTiO_3$ crystal undergoes an antiferrodistortive cubic-to-tetragonal ($O_h^1 \rightarrow D_{4h}^{18}$) structural phase transition. This behavior of PC maps well with the temperature dependence of dielectric function and electric field induced conductivity. The longevity of the PC state also shows a distinct change below $\approx$100 K. At $T > 100$ K its decay is thermally activated with an energy barrier of $\approx$36 meV, whereas at $T < 100$ K it becomes independent of temperature. We have examined the effect of electrostatic gating on the lifetime of the PC state. One nontrivial result is the ambient temperature quenching of the photoconducting state by the negative gate field. This observation opens avenues for designing a solid state photoelectric switch. The origin and lifetime of the PC state are understood in the light of field effect induced band bending, defect dynamics, and thermal relaxation processes.

DOI: 10.1103/PhysRevB.91.205117 PACS number(s): 42.70.Gi, 73.50.Pz, 71.27.+a, 74.62.Dh

I. INTRODUCTION

Understanding the physics and chemistry of complex oxides and their interfaces has been a topic of extensive study over the last few decades because of their properties, many of which are technologically very important [1]. Among many oxides $SrTiO_3$ (STO) is one of the most widely investigated, particularly from the perspective of oxide-based electronics [2,3]. Strontium titanate is a wide band gap semiconductor with an indirect gap of 3.25 eV [4], whereas its direct band gap is 3.75 eV [5]. Some fascinating characteristics of STO include high electron mobility ($\sim 10^4$ cm^2/Vs) at liquid helium temperature on electron doping [6,7], superconductivity at low temperatures in the doped state [8], electronic tunability of surface states by electrostatic gating [9], blue light emission on Ar^+-ion irradiation [3], and the observation of a two-dimensional electron gas showing magnetic and superconducting correlations at its interface with some other nonconducting perovskite oxides [6,9–17]. The many unique properties of STO have a strong bearing on its dielectric function which increases rapidly below $\simeq$120 K and also becomes electric field dependent [18,19]. The cubic perovskite structure of STO undergoes antiferrodistortive (AFD) cubic-to-tetragonal ($O_h^1 \rightarrow D_{4h}^{18}$) phase transition (PT) upon cooling below 105 K.

Many groups have studied the photoconducting state in nominally pure single crystals of $SrTiO_3$ [5,20–22] with a particular attention given to the effect of AFD-PT on photoconductivity. However, a clear connection between the two has not emerged as the very high resistance of single crystals of STO makes it difficult to examine thoroughly the dark conductivity and photoconductivity under different probing fields.

Recently, Rastogi *et al.* have studied the photoconductivity (PC) in $LaAlO_3/SrTiO_3$ and $LaTiO_3/SrTiO_3$ based heterostructures [23–26], where they found persistent photoconductivity (PPC) and suggested a role of oxygen vacancies [24,25], created in STO during the film deposition, in the stability of the PPC. These exciting results have increased interest in the studies of oxygen deficient STO even more. Oxygen vacancies can be created in STO by high temperature annealing in vacuum [27,28], using the hydrogen plasma cleaning method [29] and/or through Ar^+-ion irradiation [3,30]. In these processes, the excess electrons associated with the oxygen vacancies reduce the oxidation state of some of the Ti atoms from +4 to +3 making the material conducting.

In this report, we examine the PC behavior of $SrTiO_3$ single crystal slabs whose surface has been made conducting by ion irradiation. These studies are augmented by examination of the effects of electrostatics gating on the post-illumination recovery process. We find a strong signature of AFD-structural phase transition in the photo-induced conductivity as it undergoes an abrupt enhancement below $\approx$100 K. At room temperature, the negative gate field accelerates the recovery process of the PC state leading a complete relaxation to its ground state. However, no such acceleration was observed at 100 K. The former case offers the opportunity to create a visible blind near the UV electrostatic gate tunable photodetector.

II. EXPERIMENTAL DETAILS

The $SrTiO_3$ (100) substrates acquired from Crystal GmbH Germany had no signatures of any measurable photoconductivity upon illumination with a quartz halogen lamp. The Ar^+-ion irradiation experiments on 0.5 mm thick and optically polished STO slabs were carried out in a Kauffman type ion source operated at $\sim 8.5 \times 10^{-4}$ mbar Ar pressure. The typical acceleration voltage and ion current used for irradiation are 550 V and 1.5 mA/cm^2, respectively. The Ar^+-ion irradiation provides a direct method to fabricate electron gases within a thickness of nanometers on the surface of STO, which can be estimated on the basis of ion penetration depth (L) using

*rcb@iitk.ac.in

 ©2015 American Physical Society

the empirical formula [31]

$$L = 1.1 \times \frac{E^{2/3}W}{\rho\left(Z_i^{1/4} + Z_t^{1/4}\right)^2},$$

where, W (in amu), Z_t, and ρ are the atomic weight, atomic number, and density of the target, respectively; E is the ion energy in eV and Z_i is the atomic number of the ions. The penetration depth L of ions in our case comes out to be $\sim$35 Å. Therefore, we expect the conducting layer thickness to be of this order. The STO (100) substrates are irradiated in three different patterns; 3×3 mm^2, 1.5×5 mm^2, and 100 μm $\times$ 5 mm depending on the requirements of a specific measurement. Electrical transport measurements [mobility (μ) and sheet carrier density ($n_\square$)] were performed in the Van der Pauw configuration, where Ag/Cr electrodes were deposited on the corners of the 3×3 mm^2 irradiated STO using shadow mask, whereas the sheet resistance was measured in the standard four-probe linear geometry as well as in the Van der Pauw configuration. For the PC measurements, we have used 1.5×5 mm^2 as well as 100 μm $\times$ 5 mm irradiated channels by depositing Ag/Cr contact pads through a shadow mask, leaving a gap of $\approx$2 mm between the contact pads. Both samples showed similar PC behavior. The carrier density in irradiated channels has been tuned electrostatically by a metallic gate deposited on the back side of the STO substrate. A typical field-effect-transistor (FET) geometry of drain, source, and gate electrodes used for the PC and gate field effect measurements is shown in the inset of Fig. 2. The ultraviolet (UV) light intensity of $\sim$30 μW/cm^2 from an unfiltered quartz halogen lamp was used to illuminate the samples. The spectral profile of the lamp reported earlier [32] consists of UV range (350–400 nm), which is about 3.5% of the total integrated intensity. All temperature dependence measurements were performed in vacuum ($<2 \times 10^{-2}$ mbar) in a close cycle helium cryostat having a quartz window for optical access with $\sim$90% transmission in the spectral range of 250 nm to 850 nm. The samples degrade with time if left in the air for a few days. The results are reproducible if the samples are kept in vacuum and preferably at low temperatures.

III. RESULTS

A. Electrical transport

Figure 1 shows the sheet resistance $R_\square$, measured in a four-probe configuration of the Ar^+-ion irradiated STO at the cumulative doses of $\sim 3 \times 10^{18}$, 4.2×10^{18}, and 6×10^{18} ions/cm^2. The temperature dependent $R_\square$ measured from room temperature down to 10 K shows a metallic response with a quadratic T dependence at low temperatures. The sheet resistance at 300 K decreases from 157 $k\Omega$ to 3.5 $k\Omega$ upon increasing the dose from $\sim 3 \times 10^{18}$ ions/cm^2 to 4.2×10^{18} ions/cm^2, which can be attributed to the enhanced oxygen vacancies. However, a further increase in the dose to 6×10^{18} ions/cm^2 leads to doubling of the sheet resistance from 3.5 $k\Omega$ to 7 $k\Omega$, which may be due to excessive vacancy creation and possibly amorphization of the surface. We have therefore used the intermediate dose of $\sim 4.2 \times 10^{18}$ ions/cm^2 to irradiate the samples for all other measurements. The $R_\square(T)$ curves shown in Fig. 1 have been fitted to the expression

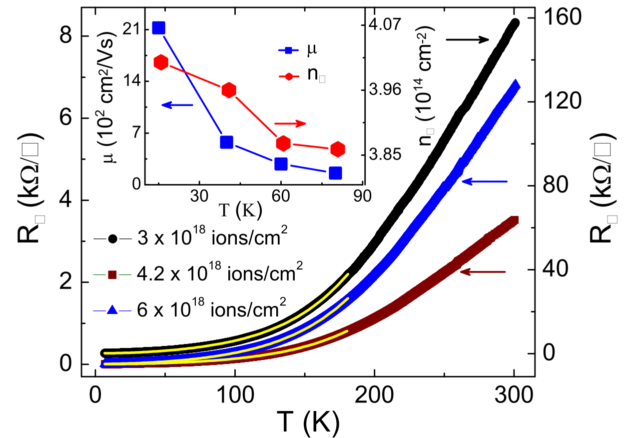

FIG. 1. (Color online) Temperature dependence of the sheet resistance $R_\square$ of three STO (100) slabs irradiated at different dosage of Ar^+ ions. The solid red lines are best fits to the expression $R_\square = R_0 + R_1T^2 + R_2T^5$, within the temperature range of 10 K to 180 K. The inset shows mobility (μ) and sheet carrier density ($n_\square$) of the sample irradiated at $\sim 4.2 \times 10^{18}$ ions/cm^2 as a function of temperature in the range 15 K to 80 K.

$R = R_0 + R_1T^2 + R_2T^5$, over the temperature range of 10 to 180 K. Here, R_0 is the residual resistance, R_1 represents the contribution from e^--e^- interactions, while R_2 originates from electron-phonon scattering [22,33]. The solid red lines shown in the figure are the fit to the data, which yields the parameters $R_1 \sim 0.5$, 0.01, and 0.02 Ω/K^2, whereas $R_2 \sim 1 \times 10^{-7}$, 2×10^{-9}, and 4×10^{-9} Ω/K^5 for the cumulative ions doses of $\sim 3 \times 10^{18}$, 4.2×10^{18}, and 6×10^{18} ions/cm^2, respectively. The dominant T^2 dependence of $R_\square$ with a weak contribution from electron-phonon scattering is evident for the metallic nature of reduced STO. The $LaTiO_3/SrTiO_3$ interface has been reported to exhibit a similar quadratic temperature dependence of $R_\square$ [24]. The temperature dependence of μ and $n_\square$ measured in Van der Pauw geometry over the range of 15 to 80 K is shown in the inset of Fig. 1. We note that the $n_\square \sim 4.0 \times 10^{14}$ cm^{-2} while μ comes out to be $\sim 21 \times 10^2$ cm^2/Vs at 15 K, which is in good agreement with the reported values at low temperatures for oxygen deficient strontium titanate [7,34]. The lower mobility seen here compared to the mobility of the $LaAlO_3/SrTiO_3$ interface ($\sim 10^4$ cm^2/Vs) [11] is presumably due to an abundance of defects in the irradiated STO and also due to a diffuse interface between the conducting and nonconducting part of STO as seen in the high resolution microscopy [35].

B. Gate effect on dark conductivity

Several source-drain current-voltage (I-V) curves of the FET structures were collected for positive and negative gate fields at various temperatures between 20 and 300 K. The conductance of the channel has a strong dependence on the polarity of the bias field similar to that seen in LTO/STO and LAO/STO interfaces [36]. The I-V curves at 20 K under different gate fields between 0 and ± 3 kV/cm are shown in Fig. 2. The curves are linear throughout the temperature range emphasizing that the contacts are ohmic and the channel is

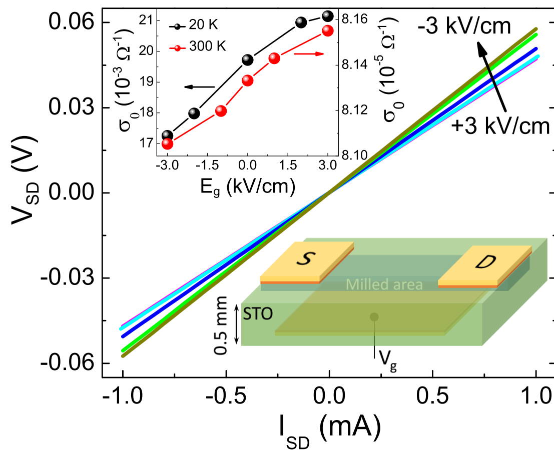

FIG. 2. (Color online) Source-drain voltage (V_{SD}) as a function of current (I_{SD}) at different gate fields varying from -3 kV/cm to $+3$ kV/cm. The data shown in the figure are taken at 20 K for the sample of ion dose $\sim 4.2 \times 10^{18}$ ions/cm^2. Sketch of a typical FET structure is shown in the lower inset. The electrodes are made of Ag/Cr bilayers deposited through a shadow mask. The upper inset shows a zero bias conductance at 20 and 300 K calculated from the slope of the I_{SD}-V_{SD} curves at the origin.

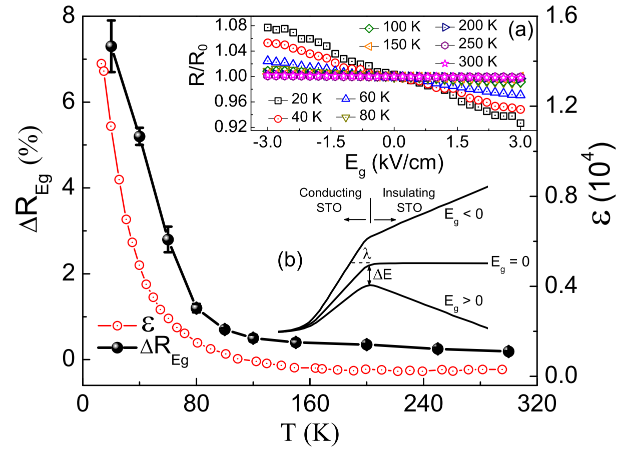

FIG. 3. (Color online) Temperature dependence of the percentage change in the resistance of a sample with an ion dose of $\sim 4.2 \times 10^{18}$ ions/cm^2; $\Delta R_{E_g}(\%) = |R(E_g = 0) - R(E_g = \pm 3)|/R(E_g = 0) \times 100$, due to gate field is shown by black spheres with error bars in the main panel of the figure. The red open circles show Ang *et al.* (Ref. [37]) data for the temperature dependence of dielectric constant (ϵ) of undoped $SrTiO_3$. The ϵ and ΔR_{E_g} grow in parallel upon lowering the temperature. Although the positive and negative gate fields change $R_\square$ in the opposite manner, the magnitude of ΔR_{E_g} in two cases differs within 10%. Inset (a) shows the normalized resistance as a function of gate field measured at several temperatures between 300 and 20 K. An illustration of band bending at the interface due to gate field is sketched in the inset (b).

metallic. We have measured the zero bias conductance, $\sigma_0 = (dI/dV)_{I_{SD}=0}$, from such linear curves for all gate fields at different temperatures from 20 to 300 K. For comparison, the 20 and 300 K data of σ_0 have been plotted in the upper inset of Fig. 2. It shows enhancement by a factor of $\sim$200 upon lowering the temperature from 300 to 20 K. The behavior of the source-drain voltage V_{SD}, as a function of gate field E_G varying from 0 to ± 3 kV/cm, is summarized in Fig. 3. For accuracy, every complete cycle of E_g going from 0 to $+3$ kV/cm to -3 kV/cm and then back to 0 has been repeated three to four times at a fixed T value. The normalized resistance R/R_0 vs E_g plots are shown in the inset (a) of Fig. 3, where R_0 is the resistance at $E_g = 0$. The curves are linear in both directions of E_g at all temperatures and no hysteresis has been observed. The increase in resistance with varying E_g from $+3$ kV/cm to -3 kV/cm indicates an n-type behavior of reduced STO, where the negative gate field reduces the charge carriers leading to increase in resistance. We have calculated the percentage change in the channel resistance defined as

$$|\Delta R_{E_g}| = \frac{|R(E_g = 0) - R(E_g = \pm 3)|}{R(E_g = 0)} \times 100,$$

where $R(E_g = 0)$ and R($E_g = \pm 3$) are the channel resistances at zero and ± 3 kV/cm gate fields, respectively. Although the channel resistance decreases (increases) as an effect of positive (negative) gate field, the difference between magnitudes of the change in channel resistance by $+3$ kV/cm and -3 kV/cm is below 10% throughout the T range. The main panel of Fig. 3 shows the temperature dependence of the percentage ΔR_{E_g}. A large enhancement in ΔR_{E_g} below $T \approx 100$ K is evident in the figure. In Fig. 3 we also show the temperature dependence of the dielectric function (ϵ) of undoped $SrTiO_3$ taken from Ang *et al.* [37]. One can clearly see a parallel in the growth of ϵ and ΔR_{E_g} upon lowering the temperature.

C. Photoinduced changes in sheet resistance

The sheet resistance of reduced STO during and after photoillumination with a broad band source of net UV flux on the sample of $\sim 30\ \mu W/\text{cm}^2$ was measured at several temperatures between 15 and 300 K. The typical acquisition time of $R_\square$(t) profiles was $\sim 2 \times 10^3$ s after turning off the illumination, while data for longer times were also recorded occasionally. We now define the normalized relative change in resistance upon photoexposure as $\Delta R_N(t) = [R_0 - R(t)]/R_0$, where R_0 is the resistance at $t = 0$ (resistance in dark), and $R(t)$ is resistance at time t. The temporal dependence of $\Delta R_N(t)$ has been shown in the inset of Fig. 4. The samples were exposed to UV light for five minutes starting from point A to point B after which the isothermal recovery of $R_\square(t)$ is monitored with t. This temporal evolution of $\Delta R_N(t)$ under illumination has two components; a rapid fall, with timescale of the order of milliseconds, followed by a gradual decrease. The post illumination recovery process also shows similar behavior with a sudden jump in R value followed by a much slower tail.

For a better understanding of the photoresponse, the net percentage change in resistance under photoillumination was defined as $\Delta R_P = \Delta R_N(t = t_1) = [R_0 - R(t = t_1)]/R_0 \times 100$, where t_1 is the time when UV light is turned off and R_0 is the resistance in the dark. The ΔR_P has been plotted as a function of T in the main graph of Fig. 4. The curve shows two very distinct regions which are well separated around 100 ere is a gradual increase in ΔR_P upon cooling from 300 to 100 K, while below 100 K the ΔR_P increases sharply. The ΔR_P (%) at 15 K is nearly twice the value at 300 K. This dramatic change

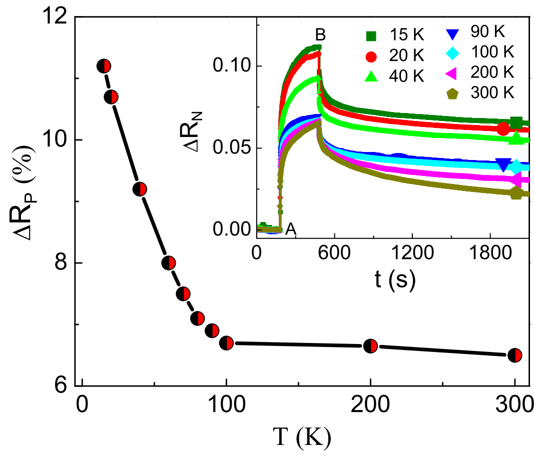

FIG. 4. (Color online) The photoinduced percentage change in resistance as a function of temperature; $\Delta R_P(\%) = [R_0 - R(t = t_1)]/R_0 \times 100$. Here t_1 is the time when UV light is turned off and R_0 is the resistance in dark (at $t = 0$). The photoinduced conductivity shows an abrupt enhancement below ~100 K. Inset shows the temporal dependence of the normalized relative change in resistance under and after photoillumination, $\Delta R_N(t) = [R_0 - R(t)]/R_0$, where R_0 is the resistance at $t = 0$ and $R(t)$ is resistance at time t, realized at various temperatures.

in the shape of ΔR_P vs T curve strongly suggests that there are two different mechanisms responsible for the different PC behavior seen below and above 100 K.

To further analyze the photo response, we monitor the post illumination recovery of the system. Figure 5 shows the behavior of $\Delta R_N(t)$ at several temperatures measured over a wide time span. As full recovery implies $\Delta R_N(t) \to 0$, it is clear from Fig. 5 that the recovery process slows down significantly at lower temperatures and becomes independent of T below ≈100 K. The decay profiles can be fitted to the

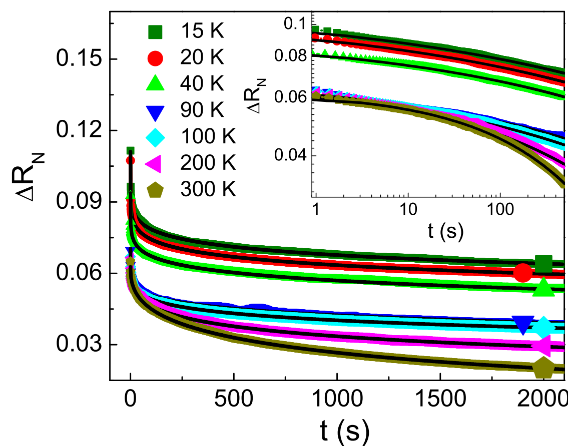

FIG. 5. (Color online) Time evolution of $\Delta R_N(t) = [R_0 - R(t)]/R_0$, after switching off photoexposure. The recovery curves show large persistent photoconductivity. The solid black lines are the best fits to the stretched exponential $\Delta R_N(t) \sim \exp[-(\frac{t}{\tau})^\beta]$. Inset shows the $\Delta R_N(t)$ profiles with fittings below $t = 500$ sec on a log-log scale.

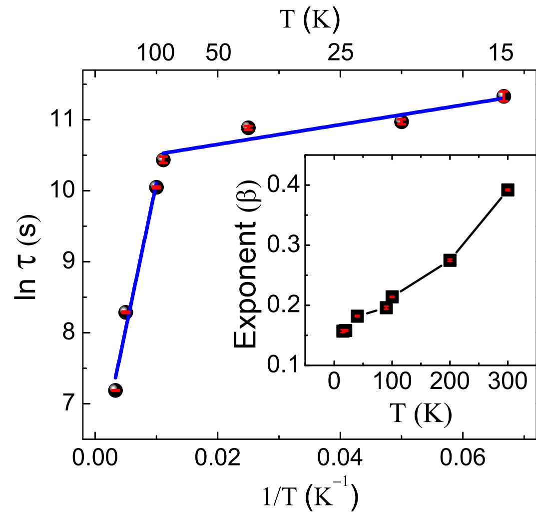

FIG. 6. (Color online) ln (τ) as a function of 1/T with error bars is plotted in the main graph whereas the temperature dependence of the decay exponent β and the error bars are shown in the inset. The T dependence of the decay time constant τ is fitted to the Arrhenius equation with two different activation energies well separated in temperature at ~100 K. The fits are shown as solid blue lines.

stretched exponential given by Kohlrausch [38]:

$$\Delta R_N(t) \sim \exp\left[-\left(\frac{t}{\tau}\right)^\beta\right].$$

Here, τ is the characteristic decay time constant of the process, while β, the decay exponent, takes a value $\leqslant 1$. Here the equality stands for the Debye relaxation processes which are governed by a single activation energy. The stretched exponential fits to the data are shown as solid black lines in Fig. 5. The temperature dependence of the parameters τ and β is shown in Fig. 6. For the relaxation time, one can notice two distinct temperature dependent regions; one at low T (below ~100 K) and the other at high T (above 100 K) indicating two activation energies, which can be expressed by the Arrhenius form [39–41]

$$\tau \sim \tau_0 \exp\left[-\frac{E_T}{K_B T}\right],$$

where the activation energy E_T is for the capture of electrons at the defect centers measured from the quasi-Fermi-level in the lowest conduction band and k_B is the Boltzmann constant. The E_T changes from ~1 meV to 36 meV as we go from the low T to the high T range. This order of magnitude difference in E_T suggests different capture mechanisms for the photogenerated carriers in different T regions.

D. Electrostatically tuned relaxation of the photoconducting state

We have discussed the electrostatic gate tuning of the dark conductivity of reduced STO in Sec. III B of this paper. Now, we will examine relaxation of the PC state under the gate field at 100 and 300 K as shown in Figs. 7 and 8, respectively. At 100 K, first the R(t) profile under and after photoillumination without any gate field was recorded. This was followed by four

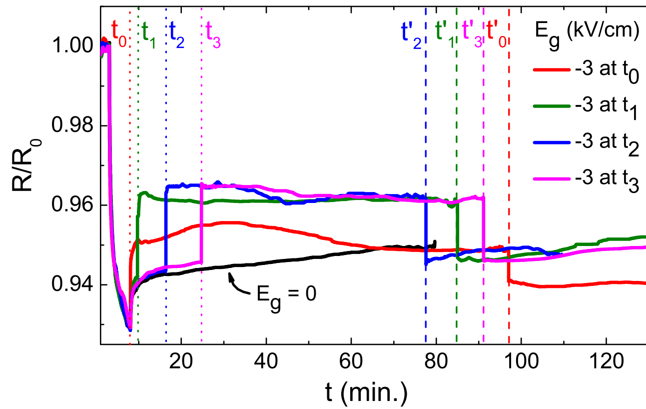

FIG. 7. (Color online) The recovery processes under negative gate field at 100 K. Black solid line is the photoresponse without any gate field and then the gate field of -3 kV/cm was applied during recovery at time $t = 0$ (t_0), 100 (t_1), 500 (t_2), and 1000 (t_3) seconds in four separate measurements, subsequently after turning off the light at t_0. The gate field applied at $t = t_0$, t_1, t_2, and t_3 was switched off at $t = t'_0$, t'_1, t'_2, and t'_3, respectively. Switching on the gate field (at $t = t_n$, where $n = 0$ to 3) leads to an abrupt increase in resistance, while there is a sudden drop in it when the gate field is turned off (at $t = t'_n$). The time scale of abrupt change in resistance is of the order of milliseconds.

separate measurements of exposure and recovery in which a -3 kV/cm gate field was applied at $t = 0$, 100, 500, and 1000 seconds after turning off the photoexposure. In each of these measurements, the sample was taken to room temperature after completion of each recovery cycle to ensure full recovery of the channel conductivity. In the 300 K measurement, the gate field applied at $t = 0$ (shown as t_0 in the figure) was switched off after relaxing the system slightly above the ground state. At this point (t'_0) the gate field was switched off and the system was allowed to come to its ground state value (R_0). Once the resistance saturates to R_0, the sample was subjected to photoexposure again with the same photon flux. The t_1, t_2, and t_3 points shown in Fig. 8(a) as dotted lines correspond to the time $t = 100$, 500, and 1000 seconds, respectively, when the gate field was applied. The dashed lines marked at t'_1, t'_2, and t'_3 in the figure mark the instant when the gate field was turned off. The results are presented in terms of normalized resistance R/R_0; R_0 being the resistance in dark, as a function of time.

At 100 K (see Fig. 7), we observe an abrupt increase in R (jump at $t = t_n$, where $n = 0 - 3$) upon application of negative E_g and then a similar drop at t'_n when the gate field is removed. However, this change in resistance is much smaller than the change caused by photoillumination. On the other hand, the effect of negative E_g on the recovery process at 300 K is remarkably different. Here the gate field not only increases the resistance abruptly at the point of application, but also accelerates the recovery process. Moreover, the identical slopes of the R/R_0 vs t curves in the time intervals ($t'_1 - t_1$), ($t'_2 - t_2$), and ($t'_3 - t_3$) suggest that the acceleration process is independent of the state of recovery. The process of recovery from the photoconducting state was also examined for several values of negative gate fields as shown in Fig. 8(b). Here the E_g was applied at the same time when the photoillumination

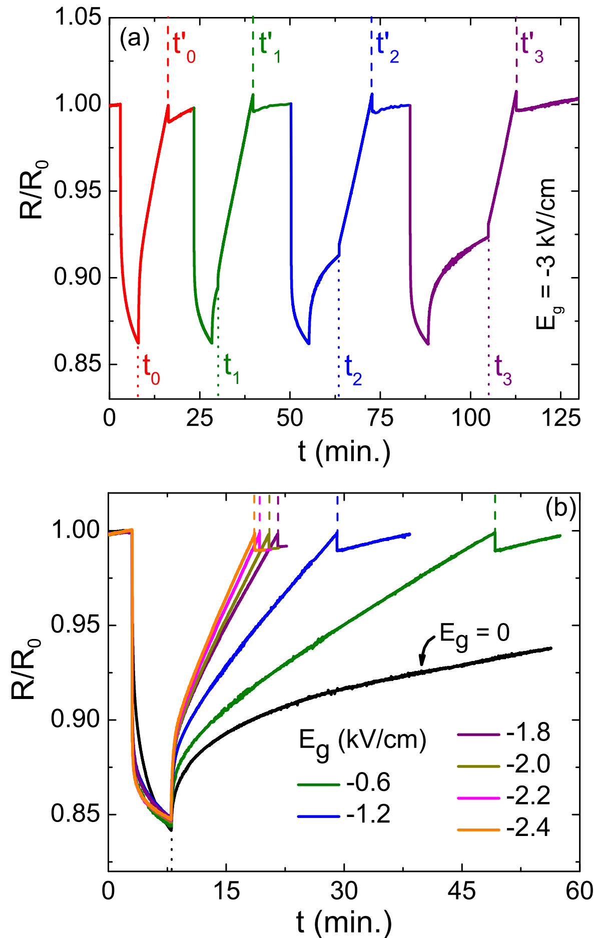

FIG. 8. (Color online) The acceleration in recovery processes by negative gate field at 300 K. (a) The gate field of -3 kV/cm applied during recovery at time $t = 0$ (t_0) and left on until t'_0. The $R_\square$ marginally exceeds its value in dark during ($t'_0 - t_0$) seconds. The sample is allowed to recover its $R_\square$ in dark after turning off the gate field and then reexposed under the same photon flux as earlier. This process is repeated for several values of t_n. (b) The dependence of the recovery process on the strength of the negative gate field. The fields were applied at the time of switching off the light as marked by the dotted line. The dashed lines indicate the point of turning off the field.

was turned off. One can clearly see an increase in acceleration to recovery with the increasing field strength.

IV. DISCUSSION

We first discuss the temperature dependence of the change in channel resistance on electrostatic gating and light exposure independently as shown in Figs. 3 and 4, respectively. The precipitous rise of ΔR_{E_g} below 100 K can be understood from the behavior of the dielectric function ϵ of STO, also shown in Fig. 3. The back gate voltage (positive/negative) changes the number of carriers (add/withdraw) at the interface and hence affects the channel conductivity (increase/decrease). Also, the induced charge carriers modify the band near the interface depending on the nature of the field as shown in the inset (b) of Fig. 3. This changes the confinement of charge carriers in the

conducting layer. As an effect of negative gate field, a depletion layer is formed which reduces the effective spatial thickness of the conducting layer leading to a decrease in conductance. If the level of conduction band edge at the interface shifts by ΔE and λ is the spatial extent over which the induced charge accumulates, then using Mott theory of field effect [42], the relative change in conductance for a semiconductor of thickness d can be written as

$$\frac{\Delta G}{G_0} = \frac{\lambda}{d}\left\{\frac{\alpha}{1+\alpha}F(-v_s) + \frac{1}{1+\alpha}F(v_s)\right\}$$
$$F(v_s) = \sum_{m=1}^{\infty}\frac{(-v_s)^m}{m m!}, \tag{1}$$

where α is the ratio of electron to hole current and v_s is the reduced surface potential $\Delta E/kT$. Also, for an exponentially decaying potential

$$\lambda = \left\{\frac{\epsilon}{4\pi e^2 N(E_F)}\right\}^{1/2}, \tag{2}$$

where $N(E_F)$ is the density of states at the Fermi level. From Eqs. (1) and (2), one can infer a square root dependence of conductance on dielectric function. Since the dielectric function of STO increases dramatically below 100 K, one would expect ΔR_{E_g} to show a similar dependence.

We now discuss the temperature dependence of ΔR_P. The gradual increase in PC upon going down from 300 to 100 K can be elucidated on the basis of e^--h^+ quasi-Fermi levels which move through the distributed levels leading to modification in the recombination kinetics [43], which increases the majority carrier lifetime upon lowering the temperature. The precipitous increase in ΔR_P below 100 K must be linked to increase in mobility (μ) or carrier density ($n_\square$) or both. Many groups have reported enhanced μ upon lowering the temperature to a value as high as $\approx 10^4$ cm^2/Vs at 10 K [6,44–46]. Such an increase in the mobility below 105 K may result from band widening due to increased overlap of 3d orbitals of Ti in the low temperature structural phase [20]. However, no abrupt change in μ is seen at the AFD PT at 105 K [6]. During this cubic to tetragonal PT, the tetragonal domains oriented along each of three original cubic axis result in the crystal with attendant twin boundaries. Recently, Kalisky *et al.* found the enhanced conductivity along these twin boundaries in $LaAlO_3/SrTiO_3$ heterointerfaces at 4 K [47]. It might be possible that the photogenerated carriers at the twin boundaries have greater mobility and hence it can contribute to the large photoresponse seen at low temperatures in irradiated STO.

Another likely mechanism for the enhanced PC is the higher photo absorption cross section in the AFD phase. The 105 K phase transition transforms the $R \rightarrow \Gamma$ indirect optical transition in the cubic phase to the much more effective direct $\Gamma \rightarrow \Gamma$ transition [21,48–50], which would lead to absorption of a good fraction of photons in the surface region of STO thereby enhancing the sheet carrier density. It is also likely that the AFD-PT changes the nature of defect states in the gap which control carrier drift and recombination processes in the system [21,43].

At this stage, it is pertinent to discuss the persistent nature of photoconductivity and its behavior under electrostatic gating.

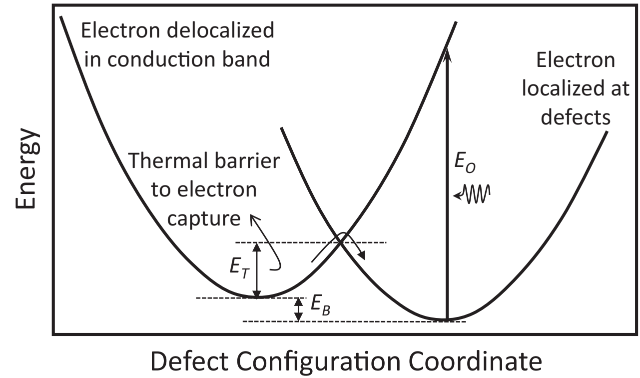

FIG. 9. Defect configuration-coordinate diagram indicating the photoexcitation of an electron by energy E_O from the defect into the conduction band, which is then captured in a thermal barrier of energy E_T. In order to relax in its ground state, the electron must have enough energy to surmount the barrier. The E_B denotes the net binding energy gained in the process of large lattice relaxation.

Theoretical approaches used to explain the phenomenon invoke either atomic scale microscopic barriers for recombination existing around defect centers with large lattice relaxation (LLR) [51], or a spatial separation of photogenerated electrons and holes by macroscopic barriers due to band bending at the surface or interfaces [52]. The ultraviolet photoemission spectroscopy studies on ion-bombarded STO show essentially zero band bending [53]. While reduced STO is prone to chemisorption of oxygen onto its surface which may lead to a nonzero band bending, the dominant role of thermal energy in PPC in the high-T region along with a substantially weak temperature dependence of the relaxation time in the low-T region strongly suggest the existence of LLR dominated PPC. To discuss this further, we invoke a defect configuration-coordinate diagram [51,54] as sketched in Fig. 9, where a photon of energy E_O promotes an electron from defect level to conduction band, which is recaptured by a thermal barrier preventing the recombination. Clearly, a photogenerated electron has to have enough thermal energy to cross this barrier for recapture onto the defect centers. The capture and thermal release model is consistent with our observation of a highly T-dependent behavior of decay time constant with an activation energy of ~36 meV in the temperature range of 300 to 100 K. However, below $\approx$100 K where the photocarriers do not have enough thermal energy to surmount the barrier, the recapture may take place by multi-phonon emission (MPE) process [55]. In this case the capture rate becomes constant as $T \rightarrow 0$. This is consistent with our observation of a nearly temperature independent τ below 100 K.

We now attempt to understand how the PPC state which survives for several hours at ambient temperature is destroyed instantaneously by a negative gate field. As the latter causes accumulation of holes at the interface of unirradiated (insulating) STO and the irradiated (conducting) STO, we believe these static charges lower the thermal barrier E_T for electron capture as shown in Fig. 9 to a sufficient degree to facilitate thermally activated recombination at 300 K. This presumably ensures quick recovery to the state existing before illumination. Moreover, as is clear from Fig. 8(b), the rate of recovery can be

controlled by the field strength. These features can be useful in optoelectronic hybrid-memory devices, where optically we can achieve the process of writing information which can then be erased electrically in a controlled fashion. On the other hand, at 100 K, where the thermal energy is too low to release the trapped electrons sitting deep in the well, the negative gate field seems not to change the recovery process as such (see Fig. 7). The hole accumulation at the interface as an effect of negative gate field leads to an abrupt increase in resistance without affecting the recovery process much. Further studies are needed to understand the behavior of recovery processes under the gate field.

V. CONCLUSIONS

In summary, the Ar^+-ion irradiated STO (100) makes an interesting two-dimensional metallic system displaying high carrier mobility at 15 K. We found evidence for the role of the anti-ferro distortive cubic-to-tetragonal phase transition in the temperature dependence of the photoinduced and electrostatic gating induced conductivity which map with the temperature dependence of the STO dielectric function. A large UV sensitive persistent photoconductivity has been observed over the temperature range of 300 to 15 K, with a relaxation time of several hours, similar to that seen in LAO-STO heterostructures. Interestingly, at 300 K, a negative gate field accelerates the post-illumination recovery process pushing the system to relax to its ground state quickly. This property has the potential for designing a solid state photoelectric switch. Our findings can be useful in understanding several unique properties of $SrTiO_3$—other oxides (such as $LaAlO_3$) interfaces, where the oxygen vacancies can significantly affect the interfacial two-dimensional electron gas.

ACKNOWLEDGMENTS

We thank A. Rastogi for helping in photoconductivity measurements and P. C. Joshi for technical help. D.K. acknowledges Indian Institute of Technology Kanpur and University Grants Commission India for financial support. R.C.B. acknowledges J. C. Bose National Fellowship of the Department of Science and Technology, Government of India.

[1] J. Mannhart and D. G. Schlom, Science **327**, 1607 (2010).
[2] K. Zhao, K.-j. Jin, Y. Huang, S. Zhao, H. Lu, M. He, Z. Chen, Y. Zhou, and G. Yang, Appl. Phys. Lett. **89**, 173507 (2006).
[3] D. Kan, R. Kanda, Y. Kanemitsu, Y. Shimakawa, M. Takano, T. Terashima, and A. Ishizumi, Appl. Phys. Lett. **88**, 191916 (2006).
[4] K. Van Benthem, C. Elsässer, and R. H. French, J. Appl. Phys. **90**, 6156 (2001).
[5] H. Zhang, L. Yan, and H.-U. Habermeier, J. Phys.: Condens. Matter **25**, 035802 (2013).
[6] O. N. Tufte and P. W. Chapman, Phys. Rev. **155**, 796 (1967).
[7] C. Lee, J. Yahia, and J. L. Brebner, Phys. Rev. B **3**, 2525 (1971).
[8] K. Ueno, S. Nakamura, H. Shimotani, A. Ohtomo, N. Kimura, T. Nojima, H. Aoki, Y. Iwasa, and M. Kawasaki, Nat. Mater. **7**, 855 (2008).
[9] M. Lee, J. R. Williams, S. Zhang, C. D. Frisbie, and D. Goldhaber-Gordon, Phys. Rev. Lett. **107**, 256601 (2011).
[10] A. Ohtomo and H. Y. Hwang, Nature (London) **427**, 423 (2004).
[11] G. Herranz, M. Basletić, M. Bibes, C. Carrétéro, E. Tafra, E. Jacquet, K. Bouzehouane, C. Deranlot, A. Hamzić, J.-M. Broto, A. Barthélémy, and A. Fert, Phys. Rev. Lett. **98**, 216803 (2007).
[12] A. Kalabukhov, R. Gunnarsson, J. Börjesson, E. Olsson, T. Claeson, and D. Winkler, Phys. Rev. B **75**, 121404 (2007).
[13] W. Siemons, G. Koster, H. Yamamoto, W. A. Harrison, G. Lucovsky, T. H. Geballe, D. H. A. Blank, and M. R. Beasley, Phys. Rev. Lett. **98**, 196802 (2007).
[14] H. Y. Hwang, Y. Iwasa, M. Kawasaki, B. Keimer, N. Nagaosa, and Y. Tokura, Nat. Mater. **11**, 103 (2012).
[15] N. Reyren, S. Thiel, A. D. Caviglia, L. Fitting Kourkoutis, G. Hammerl, C. Richter, C. W. Schneider, T. Kopp, A.-S. Rüetschi, D. Jaccard, M. Gabay, D. A. Muller, J.-M. Triscone, and J. Mannhart, Science **317**, 1196 (2007).
[16] A. Brinkman, M. Huijben, M. Van Zalk, J. Huijben, U. Zeitler, J. C. Maan, W. G. Van der Wiel, G. Rijnders, D. H. A. Blank, and H. Hilgenkamp, Nat. Mater. **6**, 493 (2007).
[17] J. Biscaras, N. Bergeal, S. Hurand, C. Grossetête, A. Rastogi, R. C. Budhani, D. LeBoeuf, C. Proust, and J. Lesueur, Phys. Rev. Lett. **108**, 247004 (2012).
[18] H.-M. Christen, J. Mannhart, E. J. Williams, and C. Gerber, Phys. Rev. B **49**, 12095 (1994).
[19] R. C. Neville, B. Hoeneisen, and C. A. Mead, J. Appl. Phys. **43**, 2124 (1972).
[20] H. Katsu, H. Tanaka, and T. Kawai, Jpn. J. Appl. Phys. **39**, 2657 (2000).
[21] F. Rossella, P. Galinetto, G. Samoggia, V. Trepakov, and L. Jastrabik, Solid State Commun. **141**, 95 (2007).
[22] K. X. Jin, B. C. Luo, Y. F. Li, C. L. Chen, and T. Wu, J. Appl. Phys. **114**, 033509 (2013).
[23] A. Rastogi, A. K. Kushwaha, T. Shiyani, A. Gangawar, and R. C. Budhani, Adv. Mater. **22**, 4448 (2010).
[24] A. Rastogi, J. J. Pulikkotil, S. Auluck, Z. Hossain, and R. C. Budhani, Phys. Rev. B **86**, 075127 (2012).
[25] A. Rastogi and R. C. Budhani, Opt. Lett. **37**, 317 (2012).
[26] A. Rastogi, J. J. Pulikkotil, and R. C. Budhani, Phys. Rev. B **89**, 125127 (2014).
[27] D. A. Muller, N. Nakagawa, A. Ohtomo, J. L. Grazul, and H. Y. Hwang, Nature (London) **430**, 657 (2004).
[28] H. Yamada and G. R. Miller, J. Solid State Chem. **6**, 169 (1973).
[29] K. S. Takahashi, D. Matthey, D. Jaccard, and J.-M. Triscone, Ann. Phys. (Berlin, Ger.) **13**, 68 (2004).
[30] F. Y. Bruno, J. Tornos, M. Gutierrez del Olmo, G. Sanchez Santolino, N. M. Nemes, M. Garcia-Hernandez, B. Mendez, J. Piqueras, G. Antorrena, L. Morellón, J. M. De Teresa, M. Clement, E. Iborra, C. Leon, and J. Santamaria, Phys. Rev. B **83**, 245120 (2011).
[31] M. Schultz and L. Klein, Appl. Phys. Lett. **91**, 151104 (2007).
[32] A. Rastogi, Ph.D. thesis, Indian Institute of Technology Kanpur, 2013, http://172.28.64.70:8080/jspui/handle/123456789/14018.

[33] G.-m. Zhao, V. Smolyaninova, W. Prellier, and H. Keller, Phys. Rev. Lett. **84**, 6086 (2000).
[34] J. H. Ngai, Y. Segal, D. Su, Y. Zhu, F. J. Walker, S. Ismail-Beigi, K. Le Hur, and C. H. Ahn, Phys. Rev. B **81**, 241307 (2010).
[35] G. Sánchez-Santolino, J. Tornos, F. Y. Bruno, F. A. Cuellar, C. Leon, J. Santamaría, S. J. Pennycook, and M. Varela, Ultramicroscopy **127**, 109 (2013).
[36] J. Biscaras, S. Hurand, C. Feuillet-Palma, A. Rastogi, R. Budhani, N. Reyren, E. Lesne, J. Lesueur, and N. Bergeal, Sci. Rep. **4**, 6788 (2014).
[37] C. Ang, R. Guo, A. S. Bhalla, and L. E. Cross, J.Appl. Phys. **87**, 3937 (2000).
[38] R. Kohlrausch, Ann. Phys. (Leipzig) **12**, 393 (1847).
[39] R. J. Nelson, Appl. Phys. Lett. **31**, 351 (1977).
[40] P. M. Mooney, J. Appl. Phys. **67**, R1 (1990).
[41] J. Y. Lin, A. Dissanayake, G. Brown, and H. X. Jiang, Phys. Rev. B **42**, 5855 (1990).
[42] N. Mott and E. Davis, *Electronic processes in non-crystalline materials*, International series of monographs on physics (Clarendon Press, Oxford, 1979).
[43] Y. T. Sihvonen, J. Appl. Phys. **38**, 4431 (1967).
[44] H. Yasunaga, J. Phys. Soc. Jpn. **24**, 1035 (1968).
[45] H. P. R. Frederikse, W. R. Thurber, and W. R. Hosler, Phys. Rev. **134**, A442 (1964).
[46] T. Ishikawa, M. Kurita, H. Shimoda, Y. Sakano, S.-y. Koshihara, M. Itoh, and M. Takesada, J. Phys. Soc. Jpn. **73**, 1635 (2004).
[47] B. Kalisky, E. M. Spanton, H. Noad, J. R. Kirtley, K. C. Nowack, C. Bell, H. K. Sato, M. Hosoda, Y. Xie, Y. Hikita, C. Woltmann, G. Pfanzelt, R. Jany, C. Richter, H. Y. Hwang, J. Mannhart, and K. A. Moler, Nat. Mater. **12**, 1091 (2013).
[48] L. F. Mattheiss, Phys. Rev. B **6**, 4718 (1972).
[49] E. Heifets, E. Kotomin, and V. A. Trepakov, J. Phys.: Condens. Matter **18**, 4845 (2006).
[50] R. A. Evarestov, E. Blokhin, D. Gryaznov, E. A. Kotomin, and J. Maier, Phys. Rev. B **83**, 134108 (2011).
[51] D. V. Lang and R. A. Logan, Phys. Rev. Lett. **39**, 635 (1977).
[52] H. J. Queisser and D. E. Theodorou, Phys. Rev. Lett. **43**, 401 (1979).
[53] V. E. Henrich, G. Dresselhaus, and H. J. Zeiger, Phys. Rev. B **17**, 4908 (1978).
[54] D. V. Lang, R. A. Logan, and M. Jaros, Phys. Rev. B **19**, 1015 (1979).
[55] B. K. Ridley, J. Phys. C: Solid State Phys. **11**, 2323 (1978).